JOURNAL OF MATERIALS SCIENCE **38** (2003) 2815–2824

Characterisation of K, Na, and Li birnessites prepared by oxidation with H_2O_2 in a basic medium. Ion exchange properties and study of the calcined products

O. PRIETO, M. DEL ARCO, V. RIVES*
Departamento de Química Inorgánica, Universidad de Salamanca, 37008-Salamanca, Spain
E-mail: vrives@usal.es

Birnessites containing Na, K or Li in the interlayer have been prepared by oxidation of Mn(II) cations with H_2O_2 in a basic medium with different alkaline cation/Mn molar ratios. The solids prepared have been characterised by elemental chemical analysis, powder X-ray diffraction, thermal analyses (differential thermal analysis and thermogravimetric analysis), FT-IR spectroscopy and surface texture assessment by adsorption of N_2 at -196°C. Crystalline birnessites are obtained for A/Mn ratios (A = K, Li) larger than 3.4, but MnO(OH) has been also identificed when such a ratio is smaller than 3.4. Ion exchange is topotactic, but is not complete for exchanging Na, K, or Mg for pre-existing Li. The solids are stable up to 400°C, and formation of spinels and solids with tunnel structures is observed at this temperature. Li-containing birnessites are transformed to $LiMn_2O_4$ spinel at 400°C, and co-crystallization of bixbyte (Mn_2O_3) is observed at higher temperatures. Bixbyte and cryptomelane are formed at 500°C for the K-containing birnessites.

1. Introduction

Birnessite manganese oxides have a layered structure, formed by [MnO_6] octahedra sharing edges, with alkaline cations and water molecules between the layers, Fig. 1 [1–11]. The formula is usually written as $A_xMnO_{2\pm y} \cdot z\ H_2O$, where A stands for the alkaline metal cation. The oxidation state of manganese is between 3.6 and 3.8 [1, 9, 12–14]. The interlayer spacing is close to 7 Å, but can increase up to 10 Å upon hydration, forming a hydrated phase known as busserite. A dehydrated form with a spacing of 5.5–5.6 Å has been also isolated [9, 12, 13, 15–17]. While birnessite contains a single layer of water molecules between the octahedra layers, busserite contains two layers of water molecules. Busserite is not stable at room temperature and is easily transformed into birnessites, although Suib *et al.* [18] have reported formation of stable busserites.

Because of the relatively easy exchange of the interlayer cations and the diversity of oxidation states of Mn in these compounds, birnessites find applications in several fields, e.g., ion exchange, batteries and heterogeneous catalysis [13, 19, 20]. Upon appropriated thermal treatments, birnessites give rise to formation of mixed oxides with tunnel or spinel structures, and these materials find wide applications; for example, Mn-Li spinels find application in rechargeable batteries [3, 12, 21–25]. Todorokite, a 3×3 spinel structure, is obtained by hydrothermal treatment of birnessites and cryptomelane, a 2×2 tunnel structure, is obtanied by calcination of birnessites [26].

We here report on the preparation and characterisation of birnessites containing K, Na or Li in the interlayer prepared by oxidation of Mn(II) cations with H_2O_2 in a basic medium. The effect of the initial A/Mn ratio on the nature of the solids obtained is studied. In addition, we study also their ion exchange ability, as well as the nature of the solids obtained by calcination. The synthesis, characterization and applications of porous manganese oxides has been recently reviewed by Suib *et al.* [27]; several methods (including precipitation, ion-exchange, hydrothermal and sol-gel routes) are discussed about their effect on the precise nature of the oxides finally formed, but the H_2O_2-oxidation process is not discussed.

2. Experimental

2.1. Preparation of the samples

All reagents were from Fluka (Switzerland) and the gases from L'Air Liquide (Spain). In a typical experiment, birnessites containing Li, Na, or K in the interlayer region have been prepared by the following procedure: 100 ml of a 0.86 M solution of AOH also 3% (v/v) H_2O_2, is dropwise added to 50 ml of a

*Author to whom all correspondence should be addressed.

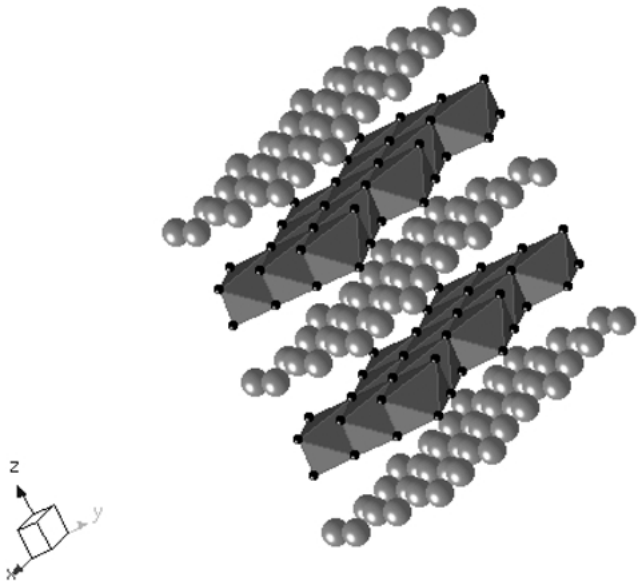

Figure 1 Scheme of the birnessite structure. Small black circles: oxygen; large circles; interlayer cations. Mn cations occupy the centre of the octahedra; interlayer water molecules have been omitted.

vigorously stirred 0.03 M solution of $Mn(NO_3)_2 \cdot 4H_2O$. The relative amounts of these solutions were changed to prepare samples with different A/Mn molar ratios. A black suspension is immediately formed, which was aged at room temperature for 1 h. The solid was separated by centrifugation and washed several times with distilled water, and finally dried in a vacuum desiccator at room temperature.

2.2. Ion exchange

This method was followed to prepare birnessites with Mg, Na, or K in the interlayer, starting from a birnessite containing Li. One gram of the birnessite was dispersed in 200 ml of a 1 M solution of KCl, NaCl or $MgCl_2$, respectively, and magnetically stirred at room temperature for 24 h, washed several times by centrifugation and separated by filtration, and finally dried in an oven at 110°C overnight.

2.3. Calcined systems

All samples prepared (parent ones and exchanged solids) were calcined in air at 400, 500, 600, 700, and 1000°C for 2 h in open air.

2.4. Naming of the samples

Samples are named as OHAX, where A stands for the interlayer alkaline cation and X for the nominal A/Mn ratio in the starting solution. Exchanged samples are named as OXLiAY, where Y corresponds to the entering cation upon ion exchange.

2.5. Characterisation of the samples

Elemental Chemical Analysis for determination of metals has been carried out by atomic absorption in Servicio General de Análisis Químico Aplicado at the University of Salamanca (Spain), after dissolving the samples in HCl, in a Mark-2 ELL-240 instrument.

Powder X-ray diffraction (PXRD) diagrams have been obtained in a D500 Siemens diffractometer with Cu Kα radiation ($\lambda = 1.54050$ Å) and graphite monochromator, 40 kV and 30 mA filament current and a scanning speed of 2° (2θ)/min. Crystalline phases have been identified by comparison with the JCPDS files [28].

Differential thermal analysis (DTA) and thermogravimetric analysis (TG) have been performed on Perkin Elmer DTA7 and TG7 instruments, respectively, connected to a Dell computer and using Pyris software. Analyses were carried out under a 20 ml/min flow of oxygen at a heating rate of 10°C/min.

Fourier Transform Infrared spectra (FT-IR) were recorded using the KBr pellet technique in a Perkin Elmer 1730 spectrometer in the 4000–400 cm^{-1} range; one hundred scans with a nominal resolution of 2 cm^{-1} were averaged to improve the signal-to-noise ratio.

Specific surface areas of the samples and their surface texture were determined from the nitrogen adsorption-desorption isotherms at −196°C, which were recorded in a Gemini instrument, from Micromeritics. The sample (ca. 0.1 g) was previously degassed at 150°C for 2 h under N_2 flow in a FlowPrep 060 instrument, also from Micromeritics. The specific surface area was determined following the BET method [29] and other methods were applied to analyze the isotherms to determine the cumulative surface area, *t*-surface, pore size distribution curves, etc., using software developed by some of us [30].

3. Results and discussion

3.1. Elemental chemical analysis

The formulae calculated for the solids prepared are given in Table I. The amount of water has been calculated from the TG curves. The H_2O/Mn ratio (between 0.71 and 1.35) is larger than that determined for similar samples, but prepared following a sol-gel method [31], although these samples had been calcined in air at 400°C. It can be also observed that the amount of water in the interlayer is larger for the Li-containing samples than for the other containing Na or K, probably because of the larger chemical potential of Li(I), which retains water more strongly.

The cation/Mn molar ratio in the solids, vs. the same ratio in the starting solutions, has been plotted in Fig. 2.

TABLE I Elemental chemical analysis (metals) and formulae of the solids prepared

Sample	Mn[a]	A[a]	Formula
OHK2.8	47.37	9.15	$K_{0.27}MnO_2 \cdot 0.77\ H_2O$
OHK3.4	44.46	9.97	$K_{0.31}MnO_2 \cdot 0.71\ H_2O$
OHK5.7	46.32	10.10	$K_{0.31}MnO_2 \cdot 0.83\ H_2O$
OHNa2.8	44.18	4.81	$Na_{0.26}MnO_2 \cdot 0.74\ H_2O$
OHNa3.4	49.34	5.91	$Na_{0.29}MnO_2 \cdot 0.74\ H_2O$
OHNa5.7	47.52	6.57	$Na_{0.33}MnO_2 \cdot 0.99\ H_2O$
OHLi2.8	47.55	1.75	$Li_{0.29}MnO_2 \cdot 1.35\ H_2O$
OHLi3.4	52.36	2.27	$Li_{0.34}MnO_2 \cdot 0.99\ H_2O$
OHLi5.7	49.97	2.16	$Li_{0.34}MnO_2 \cdot 0.96\ H_2O$

[a]% weight; A = K, Na, Li, where appropriated.

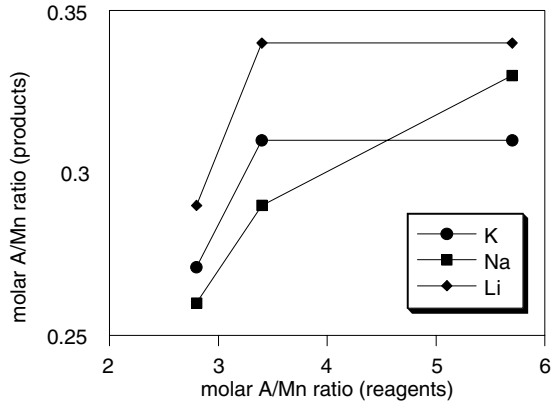

Figure 2 Relationship between A/Mn ratio in the starting solutions and in the samples prepared.

The experimental ratio increases with the initial one for low A/Mn ratios, up to A/Mn = 3.4. A further increase in the A/Mn ratio in the starting solutions does not give rise to an increase in the products for the Li or K samples; however, a further increase is observed for the Na-containing samples. In all cases, however, the A/Mn ratio in the solids is ca. one tenth of the value in the starting solutions.

The different behaviour of the Li and K samples with respect to the Na ones might be related to the simultaneous formation, in addition to birnessite, of MnO(OH) for low A/Mn ratios, but which disappears when such a ratio is increased. These results can be explained assuming that for low A/Mn ratios the excess in Mn above that required to form a stable birnessite is seggregated as MnO(OH). On the contrary, for large A/Mn ratios the birnessite is formed, and the alkaline cation in excess is removed during washing, thus leading to solids with a constant A/Mn ratio. Crystalline MnO(OH) is detected by PXRD in the Na samples with Na/Mn = 2.8 or 3.4, suggesting that transformation to the birnessite phase has not been completed, and the Na/Mn ratio in the solid increases steadily as such a ratio increases in the starting reagent solutions.

These results are similar to those previously reported by other authors [4–6], who reported a fast increase in the A/Mn ratio in the solid when the A/Mn ratio in the reagents is lower than 3.3, due to the increase in the content of the birnessite phase in the solid. For larger A/Mn ratios a steady change in such a ratio takes place, due to incorporation of alkaline cations into the interlayer space of birnessite, thus suggesting that birnessites with different A/Mn ratio can be obtained by tunning the experimental conditions during synthesis.

Suib *et al.* [32] have reported that transformation of $Mn(OH)_2$ to birnessite takes place by a topotactic reaction, with formation of intermediate β-MnO(OH) when H_2O_2 is used as an oxidant. When Mn(O(OH) is strongly oxidized the formally neutral $[MnO_3(OH)_3]$ units steadily change to $[MnO_6]$, negatively charged because of the presence of Mn(III) species. Consequently, some hydrated cations in the medium, such as K(I), can be inserted in the interlayer space to balance the negative charge of the layers. The product thus formed corresponds to a birnessite with an interlayer space close to 7 Å.

3.2. Powder X-ray diffraction

All samples synthesized exhibit a birnessite type layered structure, with an intense diffraction maximum close to 7Å due to diffraction by (001) planes; the position of this maximum slightly changes with the precise nature of the interlayer cation and the A/Mn ratio, Fig. 3.

Formation of the MnO(OH) phase in some of the samples with Li or K in the interlayer is concluded from the diffraction maximum close to 4.6 Å, together with birnessite for low A/Mn ratios in the starting solutions; for A/Mn $\geq$ 3.4 only diffraction maxima due to birnessite are recorded. Samples with Li(I) in the interlayer are very crystalline, giving rise to diffraction diagrams with intense, sharp lines, more pronounced for sample OHLi5.7. On the other side, samples with K show broader diffraction lines, suggesting a lower crystallinity of the solid. In these two series of samples the larger spacing is measured for samples with the larger nominal A/Mn ratio, because as this ratio increases the amount of alkaline cations in the interlayer also increases. Feng *et al.* [4] have reported that the highest crystallinity is obtained when Li/Mn = 3.7 and above this value crystallinity again decreases; however, such a process should be very much dependent on the specific experimental conditions during synthesis.

The 4.6 Å peak due to MnO(OH) is also observed in the PXRD diagrams of the Na-containing samples with Na/Mn $\leq$ 3.4. Contrary to what we have observed for samples prepared by a sol-gel method [31], the dehydrated phase characterised by a diffraction maximum close to 5.5 Å is not formed following this oxidation (H_2O_2) method, probably because in the sol-gel method the solid had to be calcined at 400°C to remove residues of the starting reagents used for ther sol-gel synthesis, and in the present case the samples were merely dried at room temperature. The main diffraction maximum is recorded at 7.18, 7.15, and 7.35 Å, respectively, for samples OHNa2.8, OHNa3.4, and OHNa5.7; these values are slightly larger than those recorded for the Li-containing samples, probably because of the larger ionic radius of Na(I) than Li(I). The intensity of the 7 Å peak is larger for sample OHNa3.4 than for sample OHNa2.8, probably because in this last case a portion of the manganese existing in the sample exists in the form of MnO(OH). Although for Na/Mn = 5.7 the MnO(OH) phase is no longer recorded, the diffraction maxima of birnessite are rather broad. This result is in agreement with previous reports by Feng *et al.* [4, 5]; according to these authors the maximum intensity of the 7 Å peak is recorded for Na/Mn = 4, the intensity again decreasing as this ratio progressively increases.

Quite surprisingly, the spacing for the K-containing samples is slightly smaller than that for the Na-containing samples, despite the larger ionic radius of K if compared to that of Na. The different amount of interlayer water in the samples may also account for this difference.

3.3. Thermal analyses

The behaviour of these samples upon heating depends both on the specific nature of the interlayer cation and

on its concentration. Broadly speaking, a first weight loss is recorded at rather low temperature in the TG curves, corresponding to removal of water, both weakly adsorbed on the external surface of the crystallites and between the layers. Water removal is completed at ca. 400°C. The weight loss in this temperature range has been used to calculate the amount of water in our samples (see Table I). Heating at higher temperatures leads to collapsing of the layered structure.

The DTA/TG curves of selected samples are included in Fig. 4. The DTA curves of the Li-containing samples show an exothermic effect close to 600°C due to transformation of the layered structure to the spinel; this process implies a partial reduction of Mn cations to the trivalent state, and thus takes place with oxygen release. The peak shifts towards higher temperatures as the Li/Mn ratio increases. An exothermic peak close to 560°C is also recorded for samples OHNa2.8 and OHNa3.4; at this temperature, TG curves show a small weight increase, due to oxidation of subvalent (lower than +4) Mn cations to the Mn(IV) state. On the other hand, sample OHNa5.7 exhibits a broad

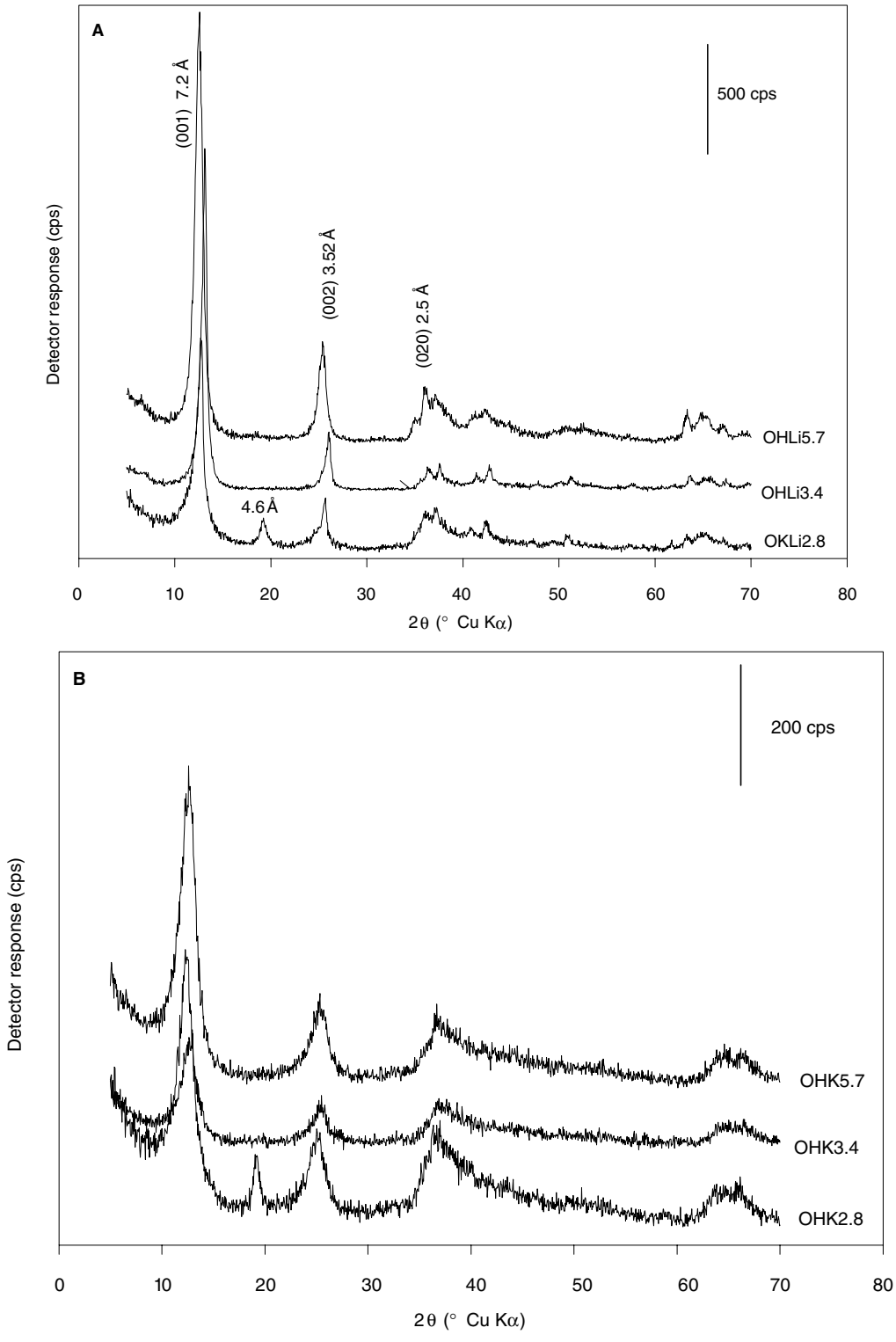

Figure 3 Powder X-ray diffraction diagrams of the samples prepared containing: (A) Li, (B) K, and (C) Na in the interlayer. Diagrams have been displaced vertically for clarity. (*Continued*)

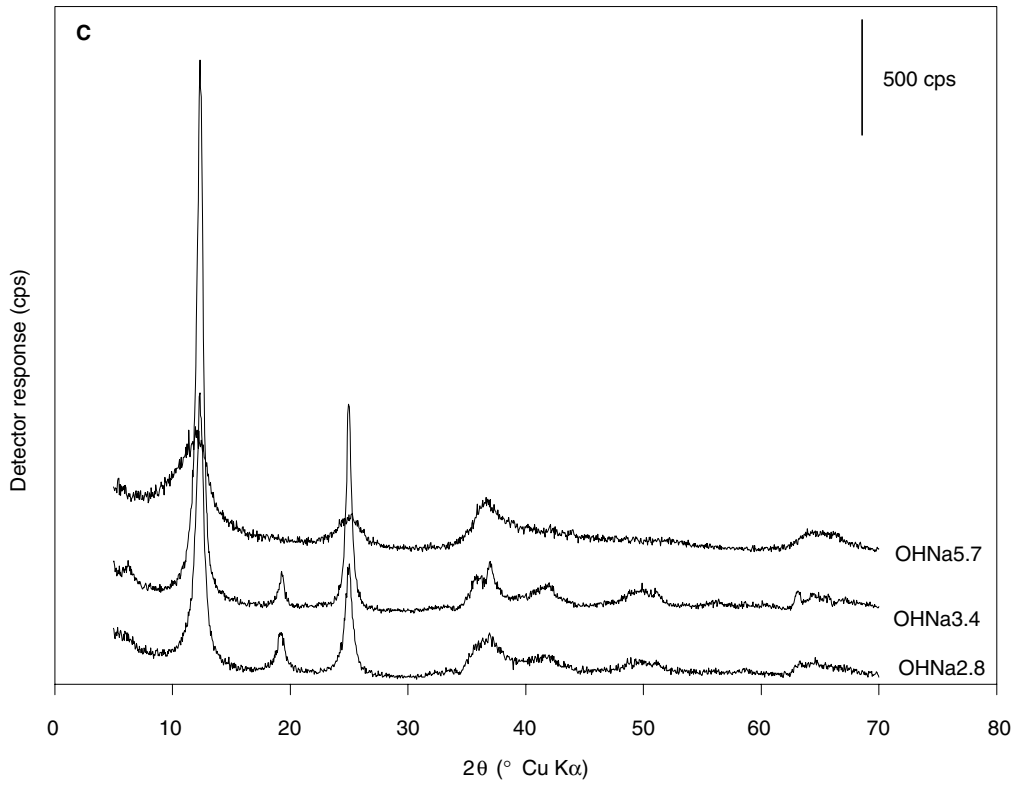

Figure 3 (*Continued*).

exothermic effect with maxima at 571 and 618°C; however, contrary to the behaviour observed for the other Na-containing samples, such exothermic effects do not correspond to any weight increase in the TG curve, and so they should correspond to a phase transformation taking place without weight change, that is, without any change in the oxidation state of the cations in the sample. Feng *et al.* [5] have ascribed an exothermic effect at this temperature to transformation from the layered birnessite structure to Mn_2O_3 and a tunnel

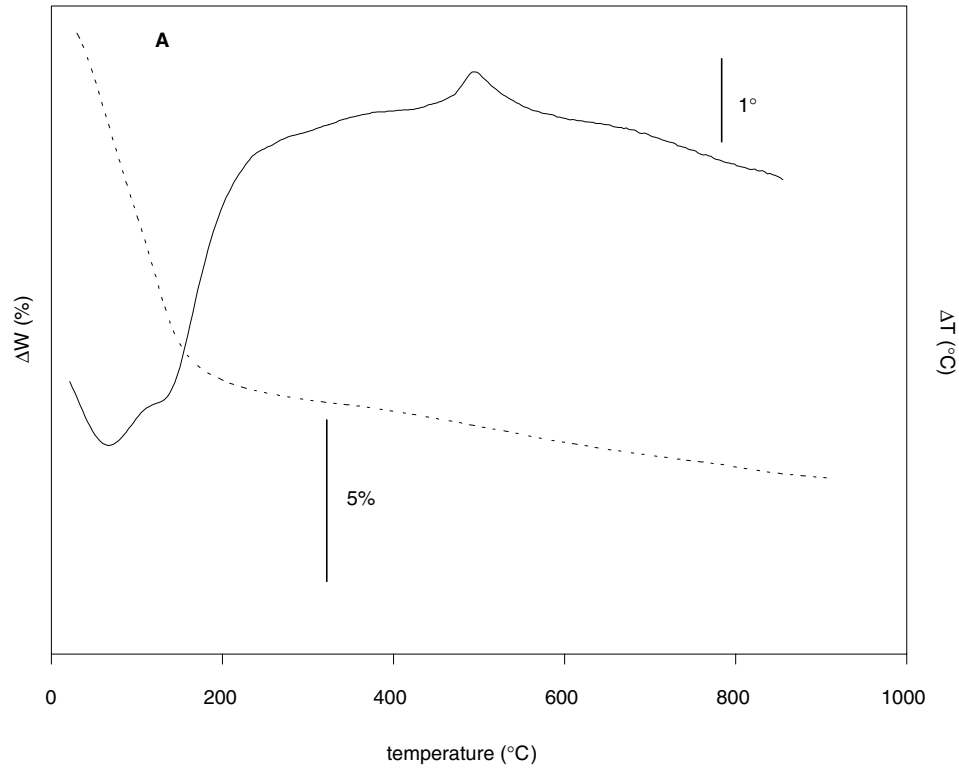

Figure 4 Differential thermal analysis (solid line, right axis) and thermogravimetric analysis (dotted line, left axis) of samples: (A) OHK3.4, (B) OHNa3.4, and (C) OHLi3.4. (*Continued*)

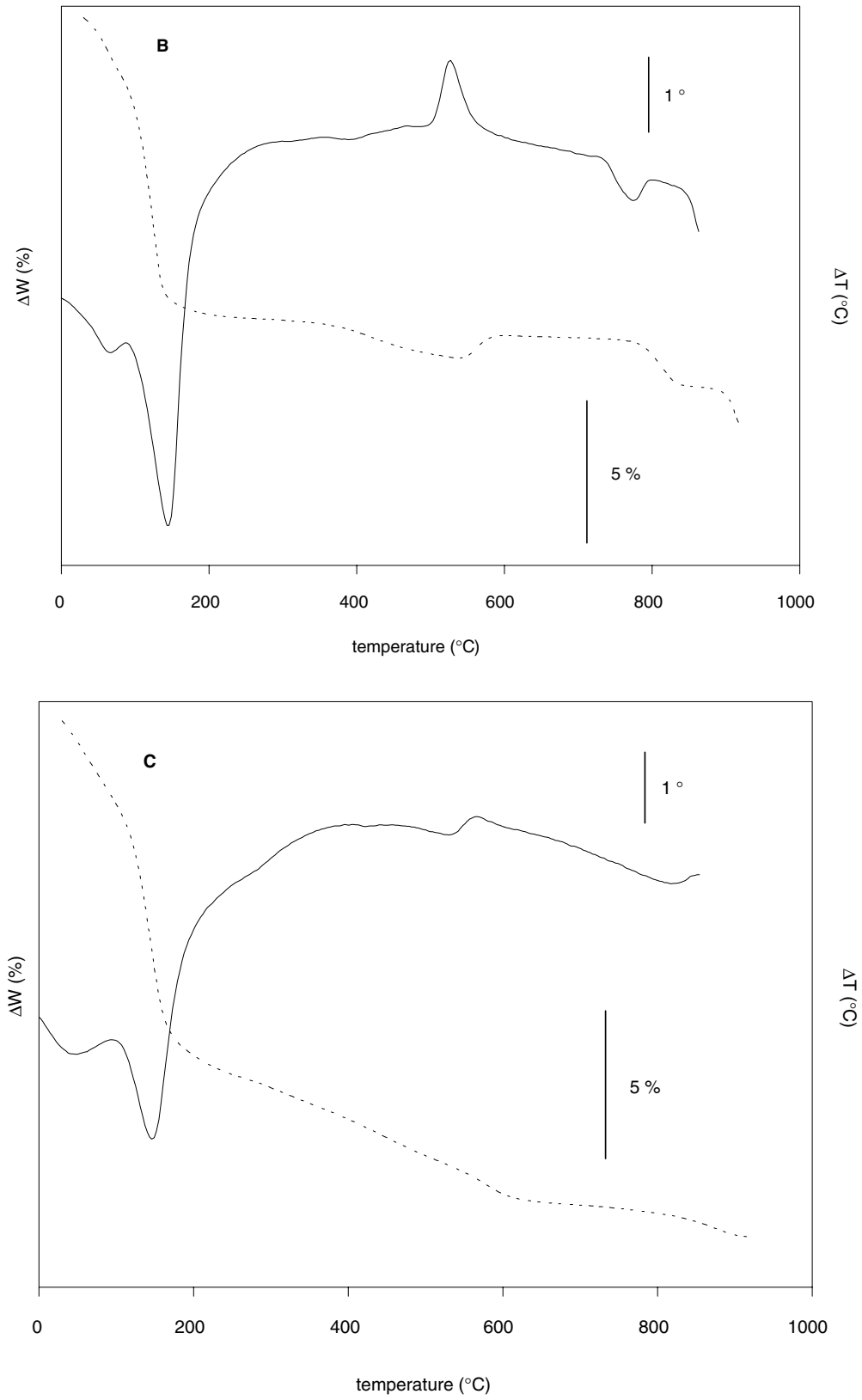

Figure 4 (*Continued*).

structure with formula $Na_{0.44}MnO_2$ or with the layered compound $Na_{0.7}MnO_2$. The specific nature of the compound formed (tunnel structured $Na_{0.44}MnO_2$ or layered $Na_{0.7}MnO_2$) accompanying Mn_2O_3 depends on the previous history of the sample. An endothermic effect is recorded for all Na samples at ca. 815°C, which intensity decreases as the Na/Mn ratio becomes smaller, and a weight loss is recorded in the TG diagram at this same temperature. This effect is due to transformation of the phases above mentioned to $NaMnO_2$ and MnO_2, which at higher temperature lead to formation of Mn_3O_4 and non-stoichiometric Na compounds. The effect due to Mn_3O_4 formation is not detected for sample OHNa5.7, suggesting that formation of the Mn spinel takes place at temperatures above the maximum limit reached in our experiments. The differences observed in

the TG and DTA diagrams for samples OHNa2.8 and OHNa3.4, if compared to those of sample OHNa5.7, may be due to the simultaneous presence of MnO(OH) detected in the former samples.

Sample OHK3.4 shows an exothermic effect centered at 545°C in its DTA curve, which is due to a partial transformation of the layered structure to cryptomelane (with simultaneous oxygen evolution) possessing a tunnel (2 × 2) structure, which has been identified by PXRD in the sample calcined at 600°C. This process takes place in two consecutive steps for sample OHK2.8 (exothemric effects at 493 and 547°C) due to the presence of MnO(OH) in this sample, which dehydrates at 370–380°C to form Mn_2O_3 [33]. An increase in the K/Mn ratio gives rise to a more stable birnessite, as collapsing of the layered structure is observed in this case at 582°C.

3.4. FT-IR spectroscopy

The FT-IR spectra of the samples prepared with Li(I), Na(I), or K(I) in the interlayer are very similar to each other, and only minor differences are found in the positions, width and splitting of the bands due to OH stretching mode of water molecules, which may be related to the different hydration degree of the interlayer and their ordering/disordering. Potter and Rosman [34] have reported a detailed study of the FTIR spectra of manganese oxides, concluding that they depend exclusively on the octahedral skeletal structure and that substitution of the interlayer cations has no major effect. Significant differences are found only in litophorite, where bands are recorded at 1000 and 900 cm^{-1} due to (Al, Li)─OH bonds, and in hollandite and cryptomelane, where differences are found in the 200–30 cm^{-1} region.

The presence of β-MnO(OH) in some of the samples, identified by PXRD in the samples with a low A/Mn ratio, might be responsible for some of the changes observed in the spectra; Suib *et al.* [32, 35] have reported that synthesis of birnessites following this oxidation method takes place topotactically from $Mn(OH)_2$ via intermediate β-MnO(OH) and, although the PXRD diagrams of fresh samples (not aged) did not show the presence of birnessite, such a phase could be identified by FT-IR spectroscopy.

A medium intense band is recorded in all spectra at ca. 3400 cm^{-1}, due to the overlapped bands of the antisymmetric and symmetric stretching modes of interlayer water molecules. Broadness of this band is due to the presence of interlayer hydrates and even water molecules directly bonded to the interlayer cations [35]. The vibration due to the deformation mode of water molecules is recorded at ca. 1620 cm^{-1}, this band being less intense than that recorded at 3400 cm^{-1}. The characteristic bands of birnessite type manganese oxides are recorded between 700 and 400 cm^{-1} [34, 35]. In our case, the bands are recorded at 515, 470, and 422 cm^{-1}, and their relative intensities change with the crystallinity of the solid; the band at 422 cm^{-1} is typical of birnessite and discriminates from other manganese oxides. A weak shoulder at 660 cm^{-1} is due to the Mn-O vibration mode.

3.5. Specific surface area and porosity

All samples displayed type II adsorption-desorption isotherms, according to the IUPAC classification [36, 37], indicating the absence of micropores. Actually, the interlayer space corresponds to micropores, but the nitrogen molecule is unable to access this space, in a similar way as previously reported for adsorption of nitrogen on hydrotalcites [38]. The isotherm shows a type H3 hysteresis loop, closing at $P/P_o \approx 0.45$, corresponding to slit like pores, probably interparticle pores. Samples are mesoporous with an average pore diameter between 20–40 Å, slightly shifting towards higher values as the A/Mn ratio increases.

The largest speceific surface areas are calculated for the Li containing samples; the values for the K samples are extremely low and below the detection limit of the system used. The change in the value of the specific surface area, determined following the BET method, with the alkaline cation content for the Na and Li samples, is shown in Fig. 5. The larger values of S_{BET} for low A/Mn ratios can be related to the presence of MnO(OH) in these samples.

The S_{BET} values for the Na samples here prepared are lower than those found previously [39] for similar samples prepared following a sol-gel method. Probably, calcination at 400°C of the sol-gel samples to remove the organic residues from the precursors lead to formation of pores and chimneys through which water vapour were evolved, thus accounting for the larger S_{BET} measured.

The values for S_{BET} decrease steadily as the Na/Mn ratio increases, but the change observed for the Li samples does not follow a linear trend; the rather high S_{BET} for sample OHLi2.8 might be due to the presence of the MnO(OH) species detected for low A/Mn ratio samples.

3.6. Ion exchange

The most crystalline sample, OHLi3.4, was selected for the ion exchange studies. Results of elemental chemical analysis (metals) for the exchanged samples are given in Table II, as well as the formula of the solids prepared with Na, K, and Mg. Exchange was not complete in any case, and ca. 10–20% of the initial Li cations remain in

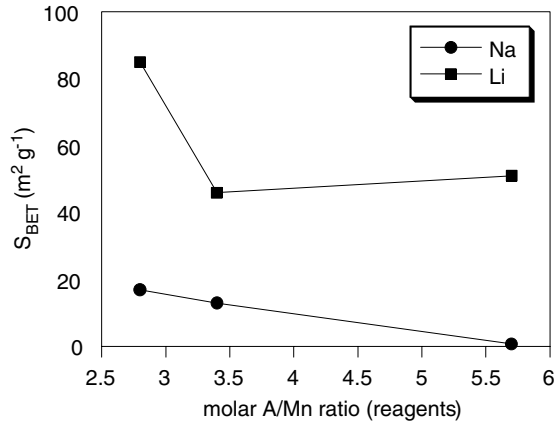

Figure 5 Change in specific surface area (BET) for Li and Na samples with the A/Mn ratio.

TABLE II Elemental chemical analysis (metals) and formulae of the solids prepared by ion exchange

Sample	Mn[a]	Li[a]	A[a]	Formula
OHLi3.4[b]	52.36	2.27	–	$Li_{0.34}MnO_2 \cdot 0.99\ H_2O$
OHLi3.4Na	51.69	0.33	6.51	$Li_{0.05}Na_{0.30}MnO_2 \cdot 0.67\ H_2O$
OHLi3.4K	49.39	0.21	10.69	$Li_{0.034}K_{0.306}MnO_2 \cdot 0.68\ H_2O$
OHLi3.4Mg	50.70	0.44	3.01	$Li_{0.068}Mg_{0.136}MnO_2 \cdot 0.99\ H_2O$

[a]% weight; A = K, Na, Li, where appropriated.
[b]original, unexchanged sample.

the exchanged solids. The amount of Mg incorporated is much larger than when the starting Li sample had been prepared by a sol-gel method [31], and no swelling of the structure (because of a buserite-like structure) is observed in any case. Feng *et al.* [4] have reported total Li/Na and Li/K exchange, but in Li/Mg exchange reached only 80%, the same value here reached; however, total Mg exchange has been reported when starting from Na birnessites [2, 26].

The water content in the exchanged samples is equal (sample OHLi3.4Mg) or smaller than in the original sample. This difference can be related to the exchange degree in these three samples or, most probably, to the same effect observed in the original samples (Table I), that is, the larger chemical potential of Mg(II) if compared to those of Na(I) and K(I): the larger chemical potential, the larger ability for water retention.

The layered structure is preserved in all cases, with only minor changes in the precise position of the diffraction maxima, especially that corresponding to planes (001), depending on the precise cation in the interlayer. From the 7.04 Å for the original OHLi3.4 sample, values of 7.10, 7.15, and 7.16 Å were measured for samples OHLi3.4Na, OHLi3,4K, and OHLi3.4Mg, respectively. Ion exchange is topotactic, preserving the layered structure. This finding is opposite to that previously reported by Feng *et al.* [4], who, upon Li/Mg exchange, obtain two crystalline phases with main maxima at 7.13 and 9.6 Å, the first one corresponding to a birnessite phase with a water layer, and the second one corresponding to a phase with two layers of water in the interlayer space, together with Mg(II) cations.

The thermal effects recorded in the TG/DTA curves for these samples are similar to those reported above for the original OHLi3.4 sample, but PXRD monitoring of the phases formed upon calcination shows changes that will be discussed below.

Incorporation of Mg leads to an increase in the S_{BET} of sample OHLi3.4Mg. However, introduction of K or Na leads to lower values; moreover, the value determined for sample OHLi3.4Na approaches that measured for the original OHNa3.4 sample. However, sample OHLi3.4K shows a S_{BET} of 23 $m^2\ g^{-1}$, much larger than that for the original OHK3.4 sample, which was below the detection limit of the instrument used.

Samples are not microporous and the pore size distribution curves indicate an average pore diameter close to 40 Å. The pore size distribution curves may explain the changes observed in the specific surface areas: while for sample OHLi3.4 pores mostly contributing to the surface area are those with diameters close to 20, 30, and 40 Å, contribution to porosity is monomodal for the exchanged samples, with an average diameter of 40 Å; the maximum adsorption capacity changes as OHLi3.4Mg > OHLi3.4K ≫ OHLi3.4Na, and S_{BET} decreases accordingly.

3.7. Calcined systems

All samples synthetised have been calcined at increasing temperatures and the nature of the new crystalline phases formed has been concluded from their PXRD diagrams. The samples are named as NAME-T, where NAME corresponds to the uncalcined sample and *T* stands for the calcination temperature, in °C.

Calcination at 400°C of the K samples does not give rise to collpasing of the layered structure and only a small shift of the (001) diffraction maximum to larger 2θ values is observed, Fig. 6, probably due to removal of interlayer water.

While for sample OHK5.7-400 peaks recorded correspond exclusively to birnessite, for the other K containing samples with lower K/Mn ratio, some diffraction maxima corresponding to cryptomelane are also observed, probably by transformation of previously existing MnO(OH).

When calcination is carried out at 500°C or above, the diagrams are similar for the three K containing samples, with destruction of the birnessite structure and formation of cryptomelane together with another K-Mn oxide identified as $K_{0.5}Mn_2O_4 \cdot 1.5H_2O$ (JCPDS file 42–1317) [28], crystallinity improving as the calcination temperature is further increased. Cryptomelane and haussmanite are formed at 1000°C.

A different behaviour is observed for the Na-containing samples. Partial dehydration takes place at 400°C, and two main maxima are recorded at 5.5 and ca. 7 Å. The first one corresponds to a dehydrated phase [15, 16, 40, 41] which is also formed during synthesis of birnessites by the sol-gel method [39]. The intensity of this dehydrated phase peak increases with the Na/Mn ratio and so, for sample OHNa5.7-400 only the peak at 5.5 Å is recorded, and that at 7 Å is absent. Formation of cryptomelane from existing MnO(OH) does not take place because of the small ionic radius of Na(I) if compared to that of K(I). These results seem to be opposite to the TG results, which showed a plateau at 400°C, suggesting that dehydration was completed at this temperature; probably, the 7 Å phase is simply formed by rehydration of the sample during handling after calcination to record the PXRD diagram.

Total collapsing of the layered structure takes place at 500°C, with formation of $Na_{0.7}MnO_2$ and $Na_2Mn_8O_{16}$, as identified from the corresponding JCPDS files. $Na_{0.7}MnO_2$ is a layered material [16, 42] crystallized in the hexagonal system; its content, in our samples, increases as the Na/Mn ratio is increased, probably because stoichiometry restrictions. $Na_2Mn_8O_{16}$ belongs to the hollandite group [8]. The same diffraction maxima are recorded after calcination at 600°C, but peaks are much sharper and intense for sample OHNa2.8, indicating a larger crystallinity of the phases formed; on the contrary, the peaks are broader for sample OHNa5.8, where also low intensity, very broad peaks,

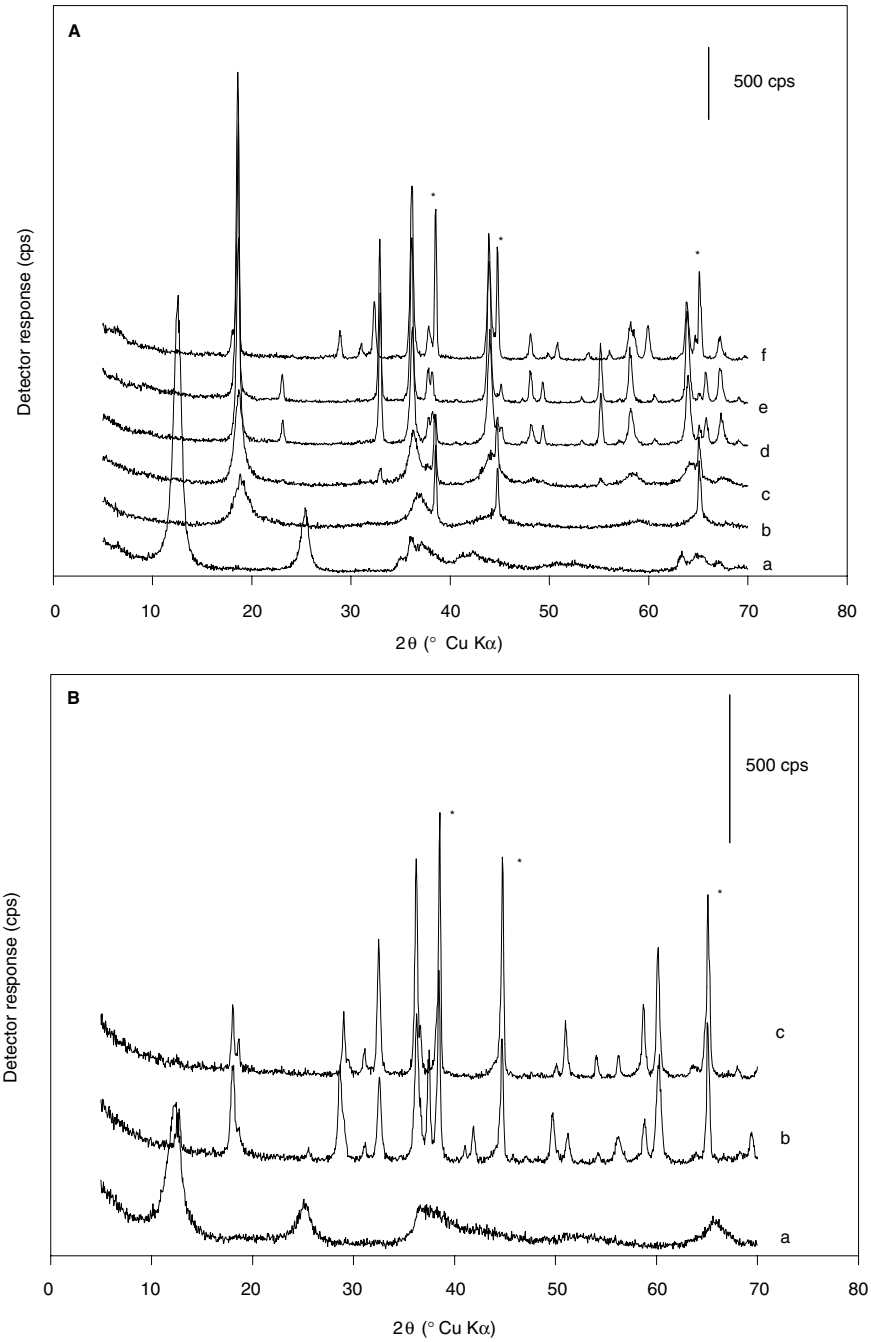

Figure 6 Powder X-ray diffraction diagram of calcined samples: (A) original OHLi5.7 sample: (a) and calcined at (b) 400°C, (c) 500°C, (d) 600°C, (e) 700°C, and (f) 1000°C. (B) Original OHLi3.4Mg sample (a) and calcined at (b) 600°C, and (c) 1000°C. Asterisk indicates diffraction by the aluminum sampleholder.

probably due to ill crystallized, mostly amorphous phases, are also recorded. In all three Na samples, calcination at 1000°C leads to sharpening of the peaks, now corresponding to haussmanite, together with weak peaks due to $Na_{0.7}MnO_2$ and $Na_2Mn_8O_{16}$.

The PXRD diagrams recorded for sample OHLi5.7 are reported in Fig. 6A. Calcination at 400°C leads to formation of a $Li_{1-x}Mn_2O_4$ spinel, which transforms at 500°C into $LiMn_2O_4$ and bixbyte, Mn_2O_3, this one being the major component after calcination at 1000°C. Although several authors have reported [12] formation of low stability (because of the small radius of Li(I) cations) cryptomelane upon calcination of Li-containing birnessites, we have not found this phase, birnessite directly forming the normal $LiMn_2O_4$ spinel.

As shown in Table II, ion exchange levels of 80–90% have been reached in our samples, and so changes in the nature of the calcined samples should be anticipated.

The large Na content in sample OHLi3.4Na leads to identification of Na-Mn-O phases upon calcination with only small contents of Li-Mn-O phases. Both $Na_2Mn_5O_{10}$ and $Na_{0.7}MnO_2$ were identified, with weak peaks due to $LiMn_2O_4$; calcination at 1000°C leads to formation of $Na_4Mn_9O_{18}$, together with Mn_3O_4 and a small conent of $LiMn_2O_4$.

When sample OHLi3.4K is calcined at 600°C the phases identified were the same as upon calcination of sample OHK3.4, with formation of cryptomelane as the single crystalline phase. However, calcination at 1000°C leads to formation of $LiMn_2O_4$, cryptomelane, $K_2Mn_4O_8$ and Mn_2O_3.

Calcination of sample OHLi3.4Mg at 600°C leads to formation of a mixed Mg-Mn oxide, $MgO \cdot Mn_2O_3$, together with small amounts of $LiMn_2O_4$ and other non-stoichiometric Mn oxides ($MnO_{1.88}$); at 1000°C the intensity of the peaks due to the mixed Mg-Mn oxide decreases, while those of the $LiMn_2O_4$ spinel increase.

The specific surface areas of the calcined samples decrease as the calcination temperature increases. In all cases, Li samples maintain the highest S_{BET} values, and microporosity does not develop in any case.

4. Conclusions

All birnessite samples prepared with a A/Mn ratio lower than 3.4 are highly crystalline, especially in the case of A = K, Li, although their crystallinity is lower than when prepared by the sol-gel method [31], which had been calcined at 400°C. Ion exchange is topotactic, the layered structure being preserved, but exchange is never complete, despite large percentages (80–90%) are reached. Thermal decomposition takes place at lower temperature than those prepared by the sol-gel method [39], and mixed crystalline phases are obtained in all cases.

Acknowledgments

Authors thank finantial support from DGES (PB96-1307-C03-01).

References

1. Q. FENG, H. KANOH, Y. MIJAY and K. OOI, *Chem. Mater.* **7** (1995) 1226.
2. *Idem.*, *ibid.* **7** (1995) 1722.
3. Q. FENG, K. YANAGISAWA and N. YAMASAKI, *J. Chem. Soc., Chem. Comm.* (1996) 1607.
4. *Idem.*, *J. Ceram. Soc. Jpn.* **104** (1996) 897.
5. Q. FENG, E. H. SUN, K. YANAGISAWA and N. YAMASAKI, *ibid.* **105** (1997) 564.
6. Q. FENG, K. YANAGISAWA and N. YAMASAKI, *J. Mater. Sci. Lett.* **16** (1997) 110.
7. *Idem.*, *J. Porous Mater.* **5** (1998) 153.
8. Q. FENG, H. KANOH and K. OOI, *J. Mater. Chem.* **9** (1999) 319.
9. S. CHING, D. J. PETROVAY, M. L. JORGENSEN and S. L. SUIB, *Inorg. Chem.* **36** (1997) 883.
10. S. CHING, J. A. LANDRIGAN, M. L. JORGENSEN, N. DUAN and S. L. SUIB, *Chem. Mater.* **7** (1995) 1604.
11. S. CHING, S. ROARK, J. L. DUAN and S. L. SUIB, *ibid.* **9** (1997) 750.
12. D. C. GOLDEN, J. B. DIXON and C. C. CHEN, *Clays Clay Miner.* **34** (1986) 511.
13. J. E. POST and D. R. VEBLEN, *Amer. Mineral.* **75** (1990) 477.
14. P. L. GOFF, N. BAFFIER, S. BACH and J. P. P. RAMOS, *J. Mater. Chem.* **4** (1994) 875.
15. P. L. GOFF, N. BAFFIER, S. BACH, J. P. P. RAMOS and R. MESSINA, *Solid State Ionics* **61** (1993) 309.
16. S. HIRANO, R. NARITA and S. NAKA, *Mater. Res. Bull.* **19** (1984) 1229.
17. B. J. ARONSON, A. K. KINSER, S. PASSERINI, W. H. SMYRL and A. STEIN, *Chem. Mater.* **11** (1999) 949.
18. J. LUO, Q. ZHANG, A. HUANG, O. GIRALDO and S. L. SUIB, *Inorg. Chem.* **38** (1999) 6106.
19. S. BACH, J. P. PEREIRA-RAMOS, N. BAFFIER and R. MESSINA, *Electrochim. Acta* **38** (1993) 1695.
20. Y. F. SHEN, S. L. SUIB and C. L. O'YOUNG, *J. Catal.* **161** (1996) 115.
21. Y. K. SUN and S. H. JIN, *J. Mater. Chem.* **8** (1998) 2399.
22. J. R. DAHN, U. V. SACKEN, M. W. JUZKOW and H. AL-JANABY, *J. Electrochem. Soc.* **138** (1991) 2207.
23. A. R. ARMSTRONG, H. HUANG, R. A. JENNIGS and P. G. BRUCE, *J. Mater. Chem.* **8** (1998) 255.
24. M. H. ROSSOUW, D. C. LILES, M. M. THACKERAY, W. I. F. DAVID and S. HULL, *Mater. Res. Bull.* **27** (1992) 221.
25. R. N. DEGUZMAN, Y. F. SHEN, E. J. NETH, S. L. SUIB, C. L. O'YOUNG, S. LEVINE and J. M. NEWSAM, *Chem. Mater.* **6** (1994) 815.
26. D. C. GOLDEN, C. C. CHEN and J. B. DIXON, *Science* **231** (1986) 717.
27. S. L. BROCK, N. DUAN, Z. R. TIAN, O. GIRALDO, H. ZHOU and S. L. SUIB, *Chem. Mater.* **10** (1998) 2619.
28. JCPDS, Joint Committee on Powder Diffraction Standards, International Centre for Diffraction Data, 1977, Pennsylvania, USA.
29. S. LOWELL and J. E. SHIELDS, "Powder Surface Area and Porosity" (Chapman and Hall, London, 1984).
30. V. RIVES, *Adsorption Sci. Technol.* **8** (1991) 95.
31. O. PRIETO, M. D. ARCO and V. RIVES, *Thermochim. Acta* **401** (2003) 95.
32. J. LUO, Q. ZHANG and S. L. SUIB, *Inorg. Chem.* **39** (2000) 741.
33. A. BLAZEK, "Thermal Analysis" (Van Nostrand Reinhold Company Ltd., London, 1973).
34. R. M. POTTER and G. R. ROSSMAN, *Amer. Mineral.* **64** (1979) 1199.
35. J. LUO, A. HUANG, S. H. PARK, S. L. SUIB and C. L. O'YOUNG, *Chem. Mater.* **10** (1998) 1561.
36. K. S. W. SING, D. H. EVERETT, R. A. W. HAUL, L. MOSCOU, R. A. PIEROTTI, J. ROUQUEROL and T. SIEMIENIEWSKA, *Pure Appl. Chem.* **57** (1985) 603.
37. A. R. PANIEGO, *An. Quim.* **35** (1989) 386.
38. V. RIVES, in "Layered Double Hydroxides: Present and Future," edited by V. Rives (Nova. Sci. Pub., Inc., New York, 2001) p. 229.
39. O. PRIETO, "Preparación, caracterización y evolución estructural con la calcinación de óxidos mixtos de manganeso," Ph.D. thesis, Universidad de Salamanca, Spain, 2001.
40. R. CHEN, P. ZAVALIJ and M. S. WHITTINGHAM, *Chem. Mater.* **8** (1996) 1275.
41. S. BACH, J. P. PEREIRA-RAMOS and N. BAFFIER, *J. Solid State Chem.* **120** (1995) 70.
42. J. P. PARANT, R. OLAZCUAGA, M. DEVALETTE, C. FOUASSIER and P. HAGENMULLER, *ibid.* **3** (1971) 1.

Received 26 December 2002
and accepted 18 April 2003